# Quantum chemical studies on molecular structure, spectroscopic (IR, Raman, UV–Vis), NBO and Homo–Lumo analysis of 1-benzyl-3-(2-furoyl) thiourea

Diego M. Gil [a,*], M.E. Defonsi Lestard [a,1], O. Estévez-Hernández [b,c], J. Duque [b,c], E. Reguera [c]

[a] INQUINOA-UNT-CONICET, Instituto de Química Física, Facultad de Bioquímica, Química y Farmacia, Universidad Nacional de Tucumán, San Lorenzo 456, T4000CAN, San Miguel de Tucumán, Argentina
[b] IMRE, Instituto de Ciencia y Tecnología de Materiales, Universidad de La Habana, Zapata y G, Vedado, La Habana, Cuba
[c] CICATA-IPN, Centro de Investigación en Ciencia Aplicada y Tecnología de Avanzada, Instituto Politécnico Nacional, Legaria 694, México, DF, Mexico

HIGHLIGHTS

- The molecular structure of 1-benzyl-3-(2-furoyl) thiourea was determined by DFT calculations.
- The vibrational frequencies and UV–visible spectrum have been calculated and correlated.
- NBO analysis was performed to evaluate the stability of the molecule.
- Weak intramolecular interactions and ellipticity were analyzed by AIM approach.
- HOMO and LUMO analysis were used to evaluate some molecular properties.

GRAPHICAL ABSTRACT
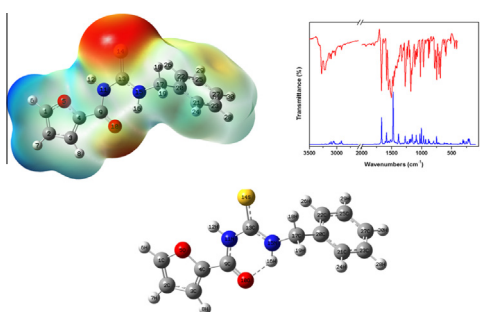
ARTICLE INFO

ABSTRACT

Vibrational and electronic spectra for 1-benzyl-3-(2-furoyl) thiourea were calculated by using density functional method (B3LYP) with different basis sets. The complete assignment of all vibrational modes was performed on basis of the calculated frequencies and comparing with the reported IR and Raman spectra for that thiourea derivative. UV–visible absorption spectra of the compound dissolved in methanol were recorded and analyzed using time dependent density functional theory (TD-DFT). The calculated values for the geometrical parameters of the title compound are consistent with the ones reported from XRD studies. The stability of the molecule, related to hyper-conjugative interactions, and electron delocalization were evaluated using natural bond orbital (NBO) analysis. Intra-molecular interactions were studied by AIM approach. The HOMO and LUMO analysis are used to determine the charge transfer within the molecule. Molecular electrostatic potential map was performed by the DFT method.

Introduction

Thiourea (NH_2CSNH_2) derivates are very useful building blocks for the synthesis of a wide range of aliphatic macromolecular and heterocyclic compounds [1–3]. These compounds could be used as ligand to form complexes with different transition metals [4–10]. Thiourea derivates usually behave as planar ligands where both, S and N atoms are donor sites able to participate in the coordination with the metal center. Substituted thioureas, however, show more diverse coordination chemistry related to their conformational isomerism, steric effects, presence of donor sites on substituent groups and intra-molecular interactions [2]. Thiourea

---

* Corresponding author. Tel.: +54 381 4311044; fax: +54 381 4248169.
   E-mail address: dmgil@fbqf.unt.edu.ar (D.M. Gil).
[1] Member of the research career of CONICET.

derivates display a wide range of biological activity including antibacterial, antifungal, antitubercular, antithyroid, antihelmintic, insecticidal, herbicidal and plant growth regulator properties [11–14]. In particular, aroylthioureas have been successful used in environmental control, as ionophores in ion selective electrodes [8].

From vibrational (IR and Raman) and electronic spectra valuable structural information is obtained. For thiourea derivatives, the active sites for complex formation with metals can be identified from such spectroscopic information [2]. However, the spectral regions where such vibrations appear are rich in signals from combination of vibration modes, overlapping of bands and complex vibration within the molecules. A comparison of IR and Raman spectra facilitates the identification of active sites [15]. A best option is found from comparative experimental and computational studies. This contribution illustrates that possibility for 1-benzyl-3-(2-furoyl) thiourea, a ligand of known crystal structure [16], whose complexes with heavy metals (Hg, Cd) have also been studied [15]. The calculated vibrational and electronic spectra were compared with the experimental ones. The computational study includes the natural bond orbital (NBO) and atoms in molecules (AIM) analysis. The HOMO and LUMO analysis have been used to elucidate information regarding ionization potential (IP), electron affinity (EA), electronegativity (χ), electrophilicity index (ω), hardness (η), softness (s) and chemical potential (μ) and all correlated. To the best of our knowledge, no analogue study has been reported for the considered thiourea derivate. The preparation and structural study of the ligand under study have been reported elsewhere [2]. UV–Vis spectra, not previously reported were collected in the course of this study using methanol solution and a Cary spectrophotometer.

Experimental details

Synthesis

The 1-benzyl-3-(2-furoyl) thiourea compound was synthesized according to a procedure reported by Otazo et al. [8]. In the synthesis the furoyl chloride was converted into furoyl isothiocyanate and then condensing with the bencylamine. Elemental analysis for $C_{13}H_{12}N_2O_2S$; found: C (67.73%), H (4.75), N (8.23%), S (9.34%); calculated: C (67.86%), H (4.46), N (8.33%), S (9.52%).

Characterization

Infrared spectrum of the solid was recorded on a FT-IR spectrophotometer (Atti Mattson, Genesis Series) using the KBr pressed disk technique in the range of 4000–400 cm^{-1} in transmission mode with 10 scans at a resolution of 2 cm^{-1}. Raman spectrum was collected by a capillary sample technique on a Perkin Elmer system 2000 NIR-FT-RAMAN and a Lexel model 98 krypton ion laser (λ = 647.1 nm). The laser power at the sample surface was restricted to 40 mW. The spectral band pass of the Raman spectrometer was 4 cm^{-1} and the 90° configuration used with an incidence angle of 60° on the metal surface when taking surface-enhanced Raman scattering (SERS). The UV–Vis spectrum in methanol was recorded at room temperature in the 250–700 nm wavelength range using a Cary 50 spectrophotometer. Sample was placed in quartz cuvette (1 cm path length).

Computational details

Theoretical calculations were performed using the program package Gaussian 03 [17]. Geometry optimizations were performed at DFT levels using the 6-31G(d,p), 6-311++G(d,p) and 6-311++G(3df,3pd) basis sets. DFT calculations were performed using Becke's three-parameter hybrid exchange functional [18] (B3) combined with both the Lee–Yang–Parr gradient-corrected correlation functional [19] (LYP). All calculations were performed using standard gradient techniques and default convergence criteria. The stability of the optimized geometries was confirmed by wavenumber calculations, which gave positive values for all the obtained wavenumbers. The vibrational modes were assigned by means of visual inspection using the Gaussview 05 program [20]. A comparison was performed between the theoretically calculated frequencies and the experimentally measured frequencies.

The prediction of Raman intensities was carried out by following the procedure outlined below. The Raman activities (S_i) were calculated by Gaussian 03 and converted to relative Raman intensity (I_i) using the following relation from the basic theory of Raman scattering [21]:

$$I_i = \frac{f(v_o - v_i)^4 S_i}{v_i[1 - \exp(-hcv_i/kT)]} \tag{1}$$

where v_o is the laser exciting wavenumber in cm^{-1} (in this work, we have used the excitation wavenumber v_o = 15453.5 cm^{-1}, which corresponds to the wavelength of 647.1 nm of the laser), v_i the vibrational wavenumber of the ith normal mode (in cm^{-1}), h, c and k are universal constants, and f is the suitably chosen common scaling factor for all the peaks intensities (10^{-12}).

A natural bond orbital (NBO) calculation was performed at the B3LYP/6-311++G(d,p) level using the program NBO 3.1 [22] as implemented in Gaussian 03 package. This analysis were performed in order to understand various second order interactions between the filled orbitals of one subsystem and vacant orbitals of another subsystem, in order to have a measure of the intramolecular delocalization of hyper-conjugation. The topological properties of the electron density at the bond critical points (BCP) have been characterized using the atoms in molecules (AIM) at the B3LYP/6-311++G(d,p) level by using the AIM2000 code [23,24]. The molecular electrostatic potential (MEP) of the title compound is illustrated and evaluated.

The molecular properties such as ionization potential, electronegativity, chemical potential, chemical hardness, softness and global electrophilicity index have been deduced from HOMO–LUMO analysis employing B3LYP/6-311++G(d,p) method. In order to understand the electronic properties, the theoretical UV–visible spectra have been computed by TD-DFT method with 6-311++G(d,p) basis sets for gas phase and solvent (methanol) effect also has been taken into consideration by implementing IEFPCM model on same level of theory.

Results and discussion

Quantum chemical calculations

Molecular structure

Fig. 1 shows the optimized molecular structure of the title compound calculated at B3LYP/6-311++G(d,p) level of theory. The dihedral angles C(4)–C(9)–N(11)–C(13) and N(11)–C(13)–N(15)–C(17) are 179.5° and −179.3°, respectively indicating that in the molecule, the thiourea group is essentially planar. The torsion angles C(13)–N(11)–C(9)–O(10), C(9)–N(11)–C(13)–N(15) and S(14)–C(13)–N(11)–C(9) are −0.52°, 0.881° and −179.1°, respectively showing that the conformation of the molecule with respect to the thiocarbonyl and carbonyl moieties is twisted. The optimized geometrical parameters calculated at B3LYP method with 6-31G(d,p), 6-311++G(d,p) and 6-311++G(3df,3pd) basis sets are shown in Table 1. These results are compared with the values reported by X-ray diffraction methods for the title compound [16]. The difference in experimental and calculated geometrical
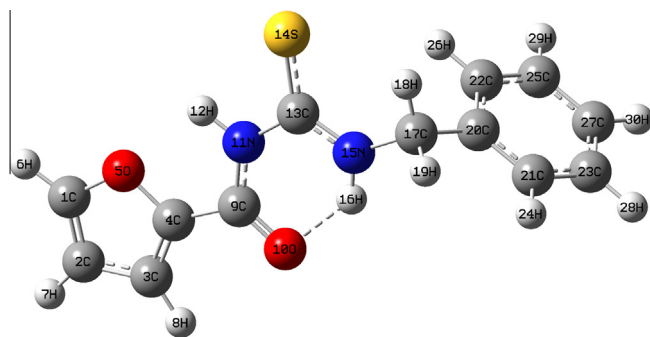
Fig. 1. Optimized molecular structure of 1-benzyl-3-(2-furoyl) thiourea calculated at B3LYP/6-311++G(d,p) level.

parameters comes from the environment of the compound. It is clear that the experimental results belong to solid phase and the theoretical calculations have been performed in gas phase and the intermolecular interactions are not taken into account. In the crystal structure reported by Pérez et al. the compound crystallizes in the tetragonal crystal system and its crystal structure is stabilized by intermolecular interactions such as N–H⋯S and N–H⋯O hydrogen bonding [16]. The bond lengths C=O and C=S of the carbonyl and thiocarbonyl groups calculated at B3LYP/6-311++G(d,p) level are 1.227 and 1.678 Å, respectively and they have typical double-bond character. However, the C–N bond lengths for the title molecule are all shorter than the average single C–N bond length (1.472 Å). These results are in agreement with the expected delocalization in the molecule and confirmed by the bond

Table 1
Selected geometrical parameters (bond lengths, angles and dihedral angles) for 1-benzyl-3-(2-furoyl) thiourea calculated at different levels of theory.

Parameters[a]	B3LYP			Experimental[b]
	6-31G(d,p)	6-311++G(d,p)	6-311++G(3df,3pd)	
Bond lengths (Å)				
O(5)–C(1)	1.359	1.357	1.353	1.363
C(1)–C(2)	1.365	1.362	1.359	1.342
C(2)–C(3)	1.426	1.426	1.423	1.420
C(3)–C(4)	1.368	1.365	1.362	1.353
C(4)–O(5)	1.373	1.372	1.368	1.374
C(4)–C(9)	1.466	1.467	1.465	1.464
C(9)=O(10)	1.233	1.227	1.224	1.228
C(9)–N(11)	1.381	1.381	1.376	1.382
N(11)–C(13)	1.404	1.405	1.402	1.388
C(13)–S(14)	1.682	1.678	1.671	1.679
C(13)–N(15)	1.339	1.339	1.335	1.323
N(15)–C(17)	1.461	1.462	1.457	1.455
C(17)–C(20)	1.517	1.515	1.512	1.515
C(20)–C(22)	1.402	1.400	1.397	1.389
C(22)–C(25)	1.393	1.392	1.388	1.384
C(25)–C(27)	1.398	1.396	1.392	1.381
C(27)–C(23)	1.394	1.392	1.388	1.379
C(23)–C(21)	1.397	1.395	1.392	1.388
C(21)–C(20)	1.398	1.396	1.392	1.390
Bond angles (°)				
C(1)–O(5)–C(4)	106.8	106.9	106.9	105.8
O(5)–C(1)–C(2)	110.6	110.5	110.6	110.7
O(5)–C(4)–C(3)	110.0	109.9	109.9	110.6
C(1)–C(2)–C(3)	106.2	106.3	106.3	107.0
C(2)–C(3)–C(4)	106.3	106.3	106.4	105.9
C(4)–C(9)=O(10)	120.9	120.9	120.9	120.6
C(4)–C(9)–N(11)	114.7	114.6	114.7	115.5
O(10)=C(9)–N(11)	124.5	124.4	124.4	123.9
C(9)–N(11)–C(13)	128.9	129.2	129.2	128.4
N(11)–C(13)–S(14)	117.7	117.7	117.6	118.5
N(11)–C(13)–N(15)	115.2	115.4	115.3	116.8
S(14)–C(13)–N(15)	127.2	126.9	127.1	124.7
C(13)–N(15)–C(17)	125.0	125.0	125.1	123.5
N(15)–C(17)–C(20)	112.6	112.6	112.6	114.1
C(20)–C(22)–C(25)	120.4	120.5	120.5	120.3
C(22)–C(25)–C(27)	120.2	120.2	120.2	120.9
C(25)–C(27)–C(23)	119.7	119.7	119.7	119.1
C(27)–C(23)–C(21)	119.9	119.9	119.9	120.5
C(23)–C(21)–C(20)	120.7	120.7	120.7	120.6
Dihedral angles (°)				
O(5)–C(4)–C(9)=O(10)	179.8	179.8	179.8	−179.6
C(4)–C(9)–N(11)–C(13)	179.8	179.5	179.4	176.4
C(9)–C(11)–C(13)–N(15)	−0.116	0.881	1.061	−2.20
N(11)–C(13)–N(15)–C(17)	−179.9	−179.3	−179.4	−175.3
S(14)–C(13)–N(15)–C(17)	−0.126	0.616	0.714	4.40
N(15)–C(17)–C(20)–C(21)	−115.1	−115.2	−115.2	−155.8
C(17)–C(20)–C(21)–C(23)	−179.5	−179.5	−179.6	−175.5
C(20)–C(21)–C(23)–C(27)	−0.194	−0.139	−0.126	−0.80
C(20)–C(22)–C(25)–C(27)	−0.112	−0.118	−0.079	−0.20
Hydrogen bond distance (Å)				
N(15)–H⋯O(10)	1.863	1.888	1.876	2.00

[a] See Fig. 1 for atoms numbering scheme.
[b] Experimental values taken from Ref. [16].

angles C(9)–N(11)–C(13) = 129.2° and C(13)–N(15)–C(17) = 125.0°. These angles show a sp^2 hybridization on the N(11) and N(15) atoms. The theoretical description of molecules containing C=S fragment requires the use of highly polarized basis functions, so that a detailed investigation of the structure was carried out using the 6-311++G(3df,3pd) basis sets. The bond lengths C–C calculated were shortened between 0.003–0.004 Å and the C=O and C=S were shortened by 0.003 and 0.007 Å, respectively upon replacing the 6-311++G(d,p) basis set with 6-311++G(3df,3pd).

The thermodynamic parameters of the title compound have also computed at B3LYP method with 6-31G(d,p) and 6-311++G(d,p) basis sets. These values are presented in Table S1. The calculation of thermodynamic parameters was performed in order to get reliable data from which the relations among energy, structure and reactivity characteristics of the molecule can be obtained. Knowledge of permanent dipole moment of a molecule provides wealth of information. It can allow us to determine the conformation of the molecule. Some differences in the dipole moment were observed with different levels of theory. The combination B3LYP/6-311++G(d,p) shows a lower value of total dipole moment than the value computed at B3LYP/6-31G(d,p) level. The high value of dipole moment obtained by calculations is probably due to the influence of the phenyl and furan ring that produce a high delocalization in the structure.

NBO analysis

The natural bond orbital (NBO) calculations were performed using NBO 3.1 program as implemented in the Gaussian03 package at the B3LYP/6-311++G(d,p) level of theory. NBO analysis is a useful tool for understanding delocalization of electron density from occupied Lewis-type (donor) NBOs to properly unoccupied non-Lewis type (acceptor) NBOs within the molecule. The stabilization of orbital interaction is proportional to the energy difference between interacting orbitals. Therefore, the interaction having the strongest stabilization takes place between effective donors and effective acceptors. This bonding–antibonding interaction can be quantitatively described in terms of the NBO approach that is expressed by means of second order perturbation interaction energy $E(2)$. This energy represents the estimate of the off-diagonal NBO Fock matrix element. The stabilization energy $E(2)$ associated with i(donor) → j (acceptor) delocalization is estimated from the second order perturbation approach as given below [22]:

$$E(2) = q_i \frac{F^2(i,j)}{\varepsilon_i - \varepsilon_i} \qquad (2)$$

where q_i is the donor orbital occupancy, ε_i and ε_j are diagonal elements (orbital energies) and $F(i,j)$ is the off-diagonal Fock matrix element. The different types of donor–acceptor interactions and their stabilization energy are determinate by second order perturbation analysis of Fock matrix of 1-benzyl-3-(2-furoyl) thiourea compound. The second order perturbation theory analysis of the Fock matrix in NBO basis for the title compound is presented in Table 2. The hyper-conjugative interactions are formed by the orbital overlap between π (C–C) bond orbital to π^* (C–C) anti-bonding orbital, which results in intra-molecular charge transfer causing the stabilization of the system. These interactions can be identified by finding the increase in electron density in the anti-bonding orbital. The strong intra-molecular hyper-conjugation interaction of the π electrons of the C–C to anti C–C and C–O bond in the ring leads to stabilization of some part of the ring as can be shown in Table 2. The bond pair donor π C–C → π^* C–C and π C–C → π^* C–O give more stabilization than σ C–C → σ^* C–C, σ C–C → σ^* N–C, σ N–C → σ^* N–C and σ C–S → σ^* C–C. A very strong interaction has been observed between the lone pair LP N(15) and the π^* C(13)–S(14) with an energy of 92.96 kcal mol^{-1}. The lone pair LP N(11)

participates in LP N(11) → π^* C(9)–O(10) and LP N(11) → π^* C(13)–S(14) interactions with energies of 61.88 and 55.10 kcal mol^{-1}, respectively. The energy value of the interaction π^* C(9)–O(10) → π^* C(3)–C(4) is 123.1 kcal mol^{-1} indicating that this interaction produces a great stabilization in the molecule.

AIM approach

The quantum theory of atoms in molecules has been useful in the characterization of bonds through a topological analysis of the electronic charge density and their Laplacian at the bond critical point (BCP) [23]. In the AIM theory the nature of the bonding interaction can be determined through an analysis of the properties of the charge density, ρ, and its Laplacian $\nabla^2(\rho)$ at the BCP, and through the properties of the atoms, which are obtained by integrating the charge density over the atom orbitals [23]. The molecular graph of the title compound using the AIM program calculated at B3LYP/6-311++G(d,p) level is presented in Fig. 2. Table 3 shows the bond critical point data for 1-benzyl-3-(2-furoyl) thiourea molecule. According to the values reported in Table 3, the charge density for the C(9)–O(10), C(13)–S(14), C(9)–N(11), C(13)–N(11), C(13)–N(15) and N(15)–C(17) bond critical points are relatively high and the $\nabla^2(\rho)$ is negative. Analyzing the sign of the Laplacian, one can define the regions where the charge density is concentrated ($\nabla^2(\rho) < 0$) or depleted ($\nabla^2(\rho) > 0$). The results shown in Table 3 indicate that the charge density has been concentrated in the inter-nuclear region according with results reported

Table 2
Second order perturbation theory analysis of the Fock matrix of 1-benzyl-3-(2-furoyl) thiourea calculated using NBO analysis.

Donor (i) → acceptor (j) interaction [a]	$E(2)$[b] kcal mol^{-1}	$E(j)–E(i)$[c] (a.u.)	$F(i,j)$[d] (a.u.)
π C(1)–C(2) → π^* C(1)–C(2)	0.85	0.30	0.014
π C(1)–C(2) → π^* C(3)–C(4)	17.20	0.30	0.067
π C(3)–C(4) → π^* C(1)–C(2)	15.60	0.29	0.061
π C(3)–C(4) → π^* C(9)–O(10)	20.73	0.28	0.070
π C(9)–O(10) → π^* C(3)–C(4)	3.96	0.40	0.038
π C(9)–O(10) → π^* C(9)–O(10)	0.90	0.38	0.018
π C(13)–S(14) → π^* C(13)–S(14)	5.33	0.22	0.035
π C(20)–C(21) → π^* N(15)–C(17)	4.47	0.59	0.050
π C(20)–C(21) → π^* C(22)–C(25)	19.49	0.29	0.067
π C(20)–C(21) → π^* C(23)–C(27)	20.25	0.28	0.068
π C(22)–C(25) → π^* C(20)–C(21)	20.91	0.28	0.069
π C(22)–C(25) → π^* C(23)–C(27)	20.30	0.28	0.068
π C(23)–C(27) → π^* C(20)–C(21)	19.91	0.29	0.068
π C(23)–C(27) → π^* C(22)–C(25)	19.70	0.29	0.067
π^* C(9)–O(10) → π^* C(3)–C(4)	123.1	0.02	0.079
σ C(2)–C(3) → σ^* C(1)–H(6)	4.60	1.09	0.063
σ C(2)–C(3) → σ^* C(4)–C(9)	5.74	1.11	0.072
σ C(4)–C(9) → σ^* N(11)–C(13)	4.05	1.10	0.060
σ N (11)–H(12) → σ^* C(9)–O(10)	4.55	1.24	0.067
σ N (11)–H(12) → σ^* C(3)–N(15)	3.58	1.16	0.058
σ N (11)–C(13) → σ^* N(15)–C(17)	3.46	1.18	0.057
σ C(13)–S(14) → σ^* C(9)–N(11)	3.54	1.11	0.057
σ N (15)–H(16) → σ^* C(13)–S(14)	6.11	0.94	0.068
LP O(5) → σ^* C(1)–C(2)	2.79	1.18	0.052
LP O(5) → π^* C(1)–C(2)	27.19	0.36	0.089
LP O(5) → σ^* C(3)–C(4)	3.36	1.18	0.057
LP O(5) → π^* C(3)–C(4)	25.38	0.37	0.087
LP O(10) → σ^* C(4)–C(9)	18.80	1.85	0.132
LP O(10) → σ^* C(9)–N(11)	25.43	1.83	0.160
LP N(11) → π^* C(9)–O(10)	61.88	0.27	0.116
LP N (11) → π^* C(13)–S(14)	55.10	0.22	0.101
LP S(14) → σ^* N(11)–C(13)	14.44	1.66	0.121
LP S(14) → σ^* C(13)–N(15)	15.28	1.86	0.141
LP N(15) → π^* C(13)–S(14)	92.96	0.19	0.123

[a] See Fig. 1 for atoms numbering. LP denotes lone pair on the specified atom.
[b] $E(2)$ means energy of hyper-conjugative interactions.
[c] Energy difference between i (donor) and j (acceptor) NBO orbitals.
[d] Fock matrix element i and j NBO orbitals.
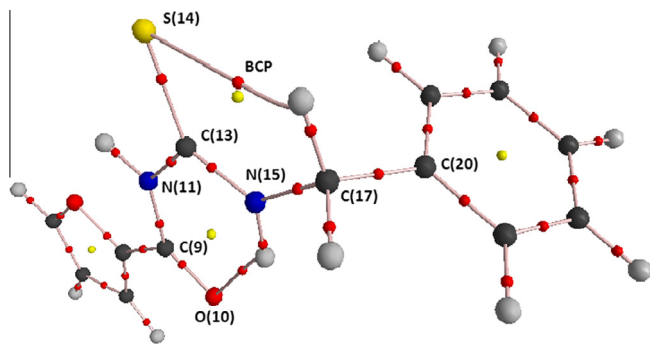
Fig. 2. Molecular graph of 1-benzyl-3-(2-furoyl) thiourea calculated at B3LYP/6-311++G(d,p) level using AIM program: bond critical points (small red spheres), ring critical points (small yellow spheres) and bond path (pink lines). (For interpretation of the references to color in this figure legend, the reader is referred to the web version of this article.)

Table 3
Bond critical point (BCP) data and BCP distances (in a.u.) to attractors calculated at B3LYP/6-311++G(d,p) level using AIM analysis.

Bond (X–Y)[a]	ρ[b]	$\nabla^2(\rho)$[b]	BCP-X	BCP-Y	Bond length (Å)
C(9)–C(10)	0.4008	−0.3517	0.7977	1.5208	1.227
C(13)–S(14)	0.2122	−0.1070	1.9235	1.2474	1.678
C(9)–N(11)	0.3077	−0.8892	0.9922	1.6172	1.381
C(13)–N(11)	0.2909	−0.8356	1.017	1.6392	1.405
C(13)–N(15)	0.3357	−0.9836	0.9479	1.5816	1.339
C(15)–C(17)	0.2522	−0.6240	1.7136	1.0486	1.462
Interaction					
O(10)···H(16)	0.03167	0.1155	2.279	1.336	1.888
S(14)···H(18)	0.01558	0.0497	3.111	1.992	2.620

[a] See Fig. 1 for atoms numbering. The first and second atom to the bond critical point (BCP).
[b] Values in a.u.

previously by Roohi et al. [24] and with calculations performed for different kind of molecules studied in our group [25–28].

The AIM methodology self-consistently partitioned any system and its properties into its atomic fragments, considering the gradient vector field of its electron density distribution. Koch et al. have proposed criteria on basis of the AIM theory to establish hydrogen bonding; the electron density at the BCP and its Laplacian are the most representative for this kind of interaction [29,30]. Moreover, since the energy density at the bond critical point (H_{BCP}) has proved to be a more sensible and appropriate index than $\nabla^2(\rho)$ to characterize the nature of hydrogen bonds [31]. The results obtained for the electron density (ρ_{BCP}), its Laplacian ($\nabla^2(\rho)_{BCP}$), electron kinetic energy density (G_{BCP}), electron potential energy density (V_{BCP}) and total electron energy density (H_{BCP}) at the bond critical points (BCPs) evaluated by means of the AIM approach at the B3LYP/6-311++G(d,p) level are presented in Table 4. The values of electron density at the BCP are in agreement with the values range reported by Koch and Popelier (0.002–0.004). Rozas et al. have suggested criteria that can be used to characterize hydrogen bonds (HB) [32]. Weak HB interactions show both $\nabla^2(\rho)_{BCP}$ and $H_{BCP} > 0$, and medium HB interactions

show $\nabla^2(\rho)_{BCP} > 0$ and $H_{BCP} < 0$, while strong HB interactions show both $\nabla^2(\rho)_{BCP}$ and $H_{BCP} < 0$. According to the values reported in Table 4, all $\nabla^2(\rho)_{BCP}$ and H_{BCP} parameters were greater than zero indicating that O(10)···H(16) and S(14)···H(18) hydrogen bonds are weak interactions.
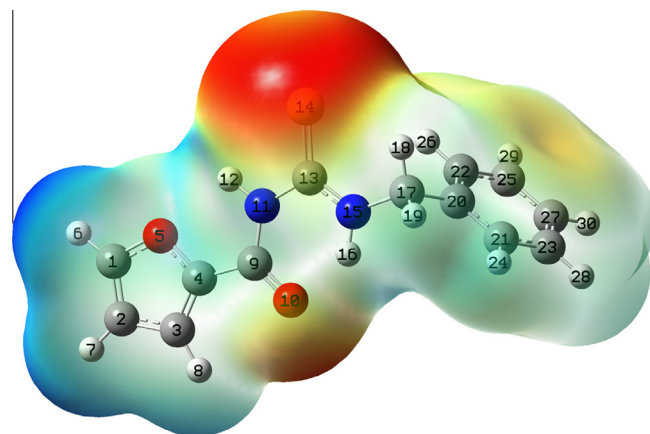
The ellipticity (ε) at the BCP is a sensitive index to monitor the π-character of bond. The ε is related to λ_1 and λ_2, which correspond to the eigen values of Hessian and defined by the relationship: $\varepsilon = (\lambda_1/\lambda_2) - 1$. The ellipticity values for bonds C(9)–C(11), C(13)–N(15), C(13)–S(14), C(1)–C(2), C(2)–C(3) and C(3)–C(4) were 0.1242, 0.1936, 0.0710, 0.3227, 0.1659, 0.3078. The lower values of ellipticity index confirm that there is electron delocalization through the corresponding atoms. However, the higher ellipticity values for C(1)–C(2) and C(3)–C(4) indicate that the electrons of these bonds are not delocalized [23].

Molecular electrostatic potential (MEP)

The molecular electrostatic potential (MEP) is related to the electron density and is a very useful descriptor in understanding sites for electrophilic and nucleophilic reactions as well as hydrogen bonding interactions [33,34]. To predict reactive sites for electrophilic or nucleophilic attacks for the investigated molecule, MEP at B3LYP/6-311++G(d,p) level optimized geometry was calculated. The different values of electrostatic potential at the MEP surface are represented by different colors: red, blue and green represent the regions of most negative, most positive and zero electrostatic potential, respectively. The negative electrostatic potential corresponds to an attraction of the proton by the aggregate electron density in the molecule (shades in red), while the positive electrostatic potential corresponds to a repulsion of the proton by the atomic nuclei (shade of blue). The negative (red and yellow) regions of MEP were related to electrophilic reactivity and the positive regions (blue) to nucleophilic reactivity. Fig. 3 shows the MEP plot for the title compound calculated at B3LYP method. From the MEP it is evident that the negative charge covers the C=O and C=S groups and the positive region is over the hydrogen of the furan ring and over the hydrogen corresponding to the benzene ring. The value of the electrostatic potential is largely responsible for the binding of a substrate to its receptor binding sites since the receptor and the corresponding ligand recognize each other at their molecular surface [35,36].

Frontier molecular orbitals (HOMO–LUMO) and global reactivity descriptors

The highest occupied molecular orbital (HOMO) energy and the lowest unoccupied molecular orbital (LUMO) energy and the

Table 4
Electron density (ρ_{BCP}), Laplacian ($\nabla^2(\rho)_{BCP}$), electron kinetic energy density (G_{BCP}), electron potential energy density (V_{BCP}) and total electron energy density (H_{BCP}) at the bond critical point (BCP) calculated by AIM analysis at B3LYP/6-311++G(d,p) level.

Interaction[a]	ρ_{BCP}	$\nabla^2(\rho)_{BCP}$	G_{BCP}	V_{BCP}	H_{BCP}
O(10)···H(16)	0.03167	0.11550	0.027270	−0.00159	0.02568
S(14)···H(18)	0.01558	0.04972	0.010931	−0.00152	0.00941

[a] See Fig. 1 for atoms numbering scheme.

Fig. 3. MEP plot of 1-benzyl-3-(2-furoyl) thiourea calculated at B3LYP/6-311++G(d,p) level.

energy gap of HOMO and LUMO are calculated at the B3LYP/6-311++G(d,p) level in order to evaluate the energetic behavior of the title molecule. The energies and the pictorial illustration of HOMO, LUMO, HOMO-1 and HOMO-2 frontier molecular orbitals are shown in Fig. 4(a). The positive and negative phase is represented in red and green color, respectively. Both HOMO and LUMO molecular orbitals play an important role in the electrical and optical properties, as well as in UV–visible spectra and chemical reactions [37]. The bioactivity and chemical activity of the molecule depends on the eigen value of HOMO, LUMO and $\Delta E_{HOMO-LUMO}$ energy gap. The HOMO represents the ability to donate an electron, LUMO as an electron acceptor represents the ability to obtain an electron. This electronic absorption corresponds to the transition from the ground state to the first excited state and is mainly described by one electron excitation from the HOMO to the LUMO frontier molecular orbital. As can be shown in Fig. 4(a), the plots reveal that the HOMO is primarily composed of C(17), N(15), S(14), N(11), O(10), C(20) and C(27) corresponding to the benzene ring. The LUMO is spread over the entire molecule except on the C atoms of the benzyl group. The HOMO-1 and HOMO-2 are involved in the electronic transitions of the title compound. The HOMO-1 is spread over the thiourea group and the HOMO-2 is spread over the entire molecule.

The energy gap, $\Delta E_{HOMO-LUMO}$ is an important value which serves as a stability index. In fact, a large HOMO–LUMO energy gap implies high molecular stability in the sense of its lower

reactivity in different chemical reactions [38,39]. The energy value of HOMO and LUMO frontier molecular orbitals with the corresponding $\Delta E_{HOMO-LUMO}$ energy gap is shown in Fig. 4(b). The HOMO–LUMO energy gap value is predicted to be 3.865 eV. This value explains the eventual charge transfer interaction with the molecule, which influences in the biological activity of the compound. The lower $\Delta E_{HOMO-LUMO}$ indicates that the title compound is reactive and less stable. A similar value of HOMO–LUMO band gap was obtained for the 2-amino-4H-chromene-3-carbonitrile indicating that the compound is highly reactive and less stable [40].

In order to understand various aspects of pharmacological sciences including drug design and the possible eco-toxicological characteristics of the drug molecules, several new chemical reactivity descriptors have been proposed. Conceptual DFT based descriptors have helped in many ways to understand the structure of molecules and their reactivity by calculating the chemical potential, global hardness and electrophilicity index. Using HOMO and LUMO orbital energies, the ionization potential (I) and electron affinity (A) can be expressed as: $I = -E_{HOMO}$ and $A = -E_{LUMO}$. Using these values we can calculate other chemical descriptors such as electronegativity $\chi = I + A/2$, chemical potential $\mu = -\chi$, hardness $\eta = I - A/2$, softness $s = 1/2\eta$ and global electrophilicity index $\omega = \mu^2/2\eta$ [41]. The global electrophilicity index was proposed by Parr et al. [42] and it measures the stabilization in energy when the system acquires an additional electronic charge from the environment. Electrophilicity encompasses both the ability of an electrophile to acquire additional electronic charge and the resistance of the system to exchange electronic charge with the environment. It contains information about both electron transfer (chemical potential) and stability (hardness) and is the better descriptor of global chemical reactivity. The energy of the frontier molecular orbitals HOMO and LUMO, $\Delta E_{HOMO-LUMO}$, electronegativity, chemical potential, hardness, softness and global electrophilicity index for the title compound calculated al B3LYP/6-311++G(d,p) level are listed in Table 5. As can be seen in Table 5, the chemical potential is negative indicating that the compound is stable and does not decompose spontaneously into its elements. The hardness signifies the resistance towards the deformation of electron cloud of chemical systems under small perturbations encountered during chemical process. Considering the chemical hardness, if a molecule has large HOMO–LUMO gap, it is a hard molecule or small HOMO–LUMO gap it is a soft molecule. One can also relate the stability of a molecule to hardness, which means that the molecule with least HOMO–LUMO gap means is more reactive. Soft systems are large and highly polarizable, while hard systems are relatively small and much less polarizable.
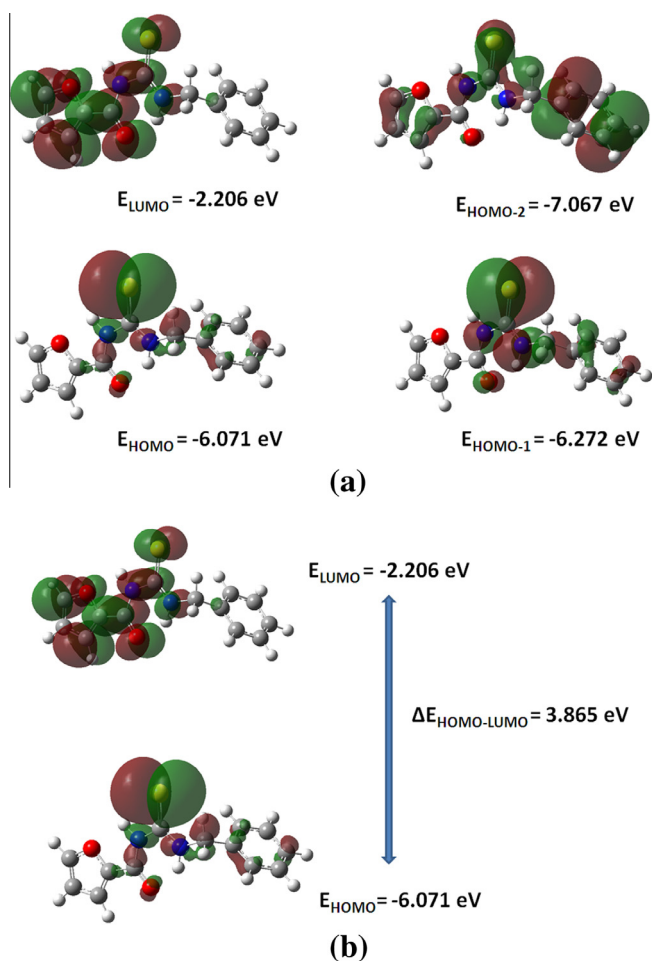
UV–visible analysis

In order to understand the nature of electronic transitions within 1-benzyl-3-(2-furoyl) thiourea molecule, TD-DFT calculations on

Fig. 4. (a) Frontier molecular orbitals (HOMO, LUMO, HOMO-1 and HOMO-2) plots of 1-benzyl-3-(2-furoyl) thiourea. (b) HOMO and LUMO plots of 1-benzyl-3-(2-furoyl) thiourea with the corresponding energies and HOMO–LUMO energy gap.

Table 5
Frontier molecular orbital energies, HOMO–LUMO gap and global reactivity descriptors for 1-benzyl-3-(2-furoyl) thiourea calculated at B3LYP/6-311++G(d,p) level.

| Molecular parameters	B3LYP/6-311++G(d,p)
E_{HOMO} (eV)	−6.071
E_{LUMO} (eV)	−2.206
$\Delta E_{HOMO-LUMO}$ (eV)	3.865
Ionization potential, IP (eV)	6.071
Electron affinity, EA (eV)	2.206
Electronegativity, χ (eV)	4.139
Chemical potential, μ (eV)	−4.139
Chemical hardness, η (eV)	1.933
Chemical softness, s (eV^{-1})	0.259
Global electrophilicity index, ω (eV)	4.431

Table 6
Theoretical electronic absorption spectra of 1-benzyl-3-(2-furoyl) thiourea calculated at B3LYP/6-311++G(d,p) level of theory in methanol solution.

Excited state	Wavelength (nm)		Excitation energies (eV)	Oscillator strengths (f)	Assignment
	Theoretical	Experimental[a]			
S1	354	–	3.499	0.0000	HOMO → LUMO
S2	303	–	4.098	0.1457	HOMO-1 → LUMO
S3	275	272	4.552	0.4947	HOMO-2 → LUMO

[a] Experimental UV–visible spectrum measured in methanol solution.
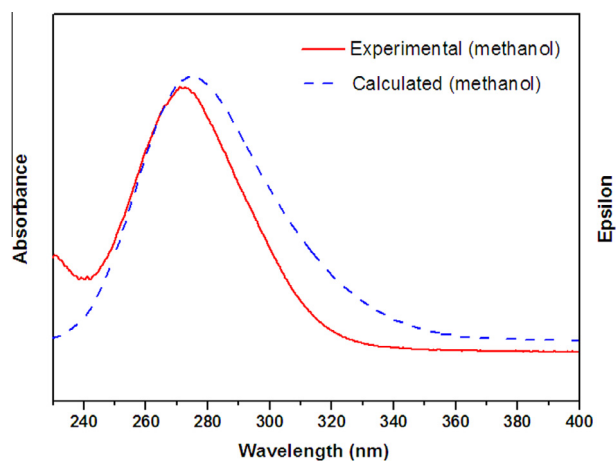
Fig. 5. Calculated and experimental UV–visible spectra of 1-benzyl-3-(2-furoyl) thiourea.

electronic absorption spectra in methanol were performed. The λ_{max} values are obtained from the UV–visible spectra analyzed theoretically with B3LYP/6-311++G(d,p) level of theory. The calculated UV absorption maxima, theoretical electronic excitation energies, and oscillator strengths are detailed in Table 6. The experimental and theoretical predicted UV–visible spectra are visualized in Fig. 5. As can be seen from Table 6, the calculated absorption maxima values for the title compound have been found to be 354, 303 and 275 nm. Oscillator strengths f is a dimensionless quantity that describes the strength of an electronic transition. Transitions with extremely low or zero f values are forbidden. The oscillator strength for the transition at 275 nm is higher in magnitude than the other transitions and its corresponding experimental value is observed at 272 nm. The maximum absorption at 272 nm is assigned to the transition from the HOMO-2 to LUMO molecular orbital. This transition is predicted to be of $\pi \to \pi^*$ nature (see Fig. 4(a)). The absorption band located at 303 nm in the calculated spectrum (f = 0.1457) is assigned to the HOMO-1 → LUMO transition ($n \to \pi^*$ nature). This band was not observed experimentally probably because it is obliterated by the much more intense absorption band located at 272 nm. The wavelength calculated at 354 nm (f = 0.0000) is mainly generated by excitations from the HOMO to LUMO molecular orbital. This band was not observed experimentally.

Vibrational analysis

The 1-benzyl-3-(2-furoyl) thiourea compound lacks of any symmetry (C_1 point group). Therefore, all 84 normal modes of vibrations are both IR and Raman active. The assignment of the observed bands in the solid state FTIR and Raman spectra of the title compound was assisted by theoretical calculations. The frequencies were calculated in the harmonic approximation at the B3LYP/6-311++G(d,p) level of theory. The experimental IR and Raman spectra are shown in Fig. 6. The simulated IR and Raman

spectra of the title molecule are presented in Figure S1. The experimental and calculated vibration frequencies are compared in Table 7 along a tentative mode assignment. The discrepancy observed between observed and calculated frequencies could be explained due to the fact that the inter-molecular interactions unavoidably present in the solid state is not taken into account in the gas phase theoretical calculations. Vibration mode frequencies calculated at B3LYP/6-311++G(d,p) level were scaled by 0.983 at wavenumbers higher than 1700 cm^{-1} and by 0.958 at wavenumbers lower than 1700 cm^{-1} to correct for theoretical error in this work [43].

Assignment of bands

N–H group vibrations. The N–H stretching vibrations generally give rise to bands at 3500–3300 cm^{-1} [44–46]. The very weak band observed in the IR spectrum at 3319 cm^{-1} is assigned to the N(11)–H stretching mode. The medium intensity band located at 3277 cm^{-1} in the IR spectrum (3278 cm^{-1} in Raman) is assigned to the N(15)–H stretching vibration. The calculated wavenumbers calculated for these modes are 3593 and 3442 cm^{-1}, respectively. As can be seen in Table 7, the N–H stretching frequency is shifted by 274 and 165 cm^{-1} in the IR spectrum from the calculated frequencies, which indicates the weakening of the N–H bond resulting in proton transfer to the neighboring oxygen (hydrogen bonding).

The strong bands located at 1514 and 1504 cm^{-1} (1514 cm^{-1} in Raman) are assigned to the CN–H in-plane bending mode. The medium intensity band observed at 709 cm^{-1} and the band located at 629 cm^{-1} in the IR spectrum are assigned to the CN–H out-of-plane bending mode.

CH$_2$ group modes. The band located at 3055 cm^{-1} in the Raman spectrum is assigned to the anti-symmetric stretching mode of the methylene group. The weak band observed in the IR spectrum
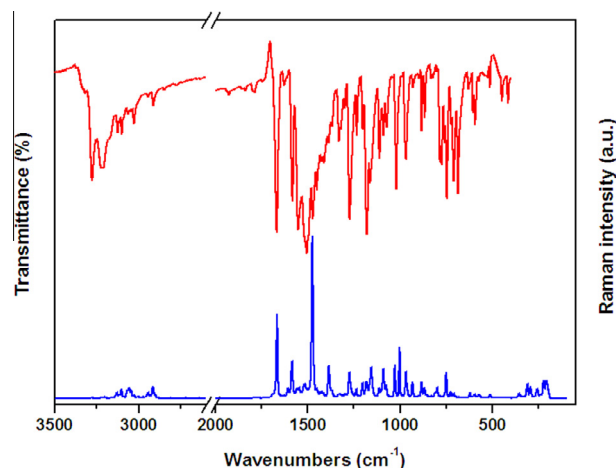
Fig. 6. Experimental IR and Raman spectra of 1-benzyl-3-(2-furoyl) thiourea in solid state.

Table 7
Observed and calculated mode frequencies (in cm^{-1}) and tentative assignments for 1-benzyl-3-(2-furoyl) thiourea vibrations.

Mode	Experimental		Calculated[c]		Tentative assignment[d,e]
	IR[a]	Raman[b]	Unscaled	Scaled	
1	3319 vw	–	3593 (52)	3532	ν N(11)–H
2	3277 m	3278 (1)	3442 (241)	3383	ν N(15)–H
3	3221 w	3225 (1)	3280 (<1)	3224	ν C(1)–H
4	3211 w	3206 (1)	3267 (2)	3211	ν C(3)–H
5	3168 sh	3165 (1)	3250 (1)	3195	ν C(2)–H
6	3138 vvw	3135 sh	3190 (17)	3136	ν C(27)–H
7	3125 vw	3129 (4)	3180 (23)	3126	ν C(23)–H
8	3113 vw	3115 (3)	3172 (8)	3118	ν C(22)–H
9	–	–	3163 (<1)	3109	ν C(25)–H
10	3100 vw	3103 (6)	3155 (7)	3101	ν C(21)–H
11	–	3055 (7)	3104 (10)	3051	ν_a CH$_2$
12	2914 w	2916 (7)	3043 (33)	2991	ν_s CH$_2$
13	1666 s	1665 (51)	1713 (266)	1684	ν C=O
14	1582 m	1584 (23)	1644 (8)	1575	ν C(21)–C(23) + ν C(22)–C(25)
15	–	1557 (7)	1626 (4)	1558	ν C(23)–C(27) + ν C(22)–C(20)
16	1550 s	1545 (8)	1621 (81)	1553	ν C(3)–C(4)
17	1514 s	1514 (9)	1590 (460)	1523	δ C(13)–N(15)–H
18	1504 vs	–	1553 (683)	1488	δ C(9)–N(11)–H
19	1495 sh	–	1527 (12)	1463	δ CCH
20	1472 m	1474 (100)	1503 (108)	1440	ν C(3)–C(4) + δ CH$_2$
21	1450 w	1452 (7)	1487 (27)	1425	δ CH$_2$
22	1426 w	1427 (5)	1484 (25)	1422	δ CCH (R2)
23	1386 w	1385 (20)	1414 (14)	1355	δ CCH (R1)
24	1367 w	1369 sh	1406 (114)	1347	ω CH$_2$ + ν C(13)–N(15)
25	1330 w	1328 (3)	1366 (157)	1346	ν C(13)–N(15)
26	1320 vw	–	1357 (21)	1300	δ CCH (R2)
27	1272 s	1273 (16)	1340 (21)	1284	ν C(21)–C(20) + ν C(21)–C(27)
28	1234 w	1236 (6)	1287 (111)	1233	ν C(4)–C(9)
29	1201 w	1202 (9)	1268 (117)	1215	$\tau\omega$ CH$_2$
30	1179 s	1182 (11)	1246 (17)	1194	δ CCH (R1) + ν C(4)–O(5)
31	1162 m	1162 sh	1223 (6)	1172	ν C(17)–C(20) + δ CCH (R2)
32	1154 sh	1155 (19)	1203 (1)	1152	δ CCH (R2)
33	–	–	1193 (136)	1143	δ COH (R1) + ν C(13)–N(11)
34	–	–	1182 (<1)	1132	δ CCH (R2)
35	1111 m	1112 (6)	1164 (102)	1115	ν C(13)–N(11) + δ COH (R1)
36	1089 w	1089 (18)	1130 (20)	1083	ν C(17)–N(15)
37	1071 w	1076 (9)	1108 (23)	1061	ν C(1)–O(5) + ν C(17)–N(15)
38	–	1057 (1)	1104 (24)	1058	δ CCH (R2)
39	–	1043 (1)	1086 (11)	1040	ν C(9)–N(11) + δ CCH (R1)
40	1019 m	1022 (20)	1050 (7)	1006	δ CCH (R2)
41	–	1002 (30)	1032 (58)	989	δ CCH (R1)
42	971 sh	–	1017 (44)	974	δ C(27)C(23)C(21) + δ C(22)C(20)C(21)
43	966 w	966 (16)	1004 (<1)	962	γ C–H (R2)
44	956 sh	959 sh	986 (<1)	945	γ C–H (R2)
45	930 vw	932 (10)	974 (33)	933	ρ CH2 + γ C–H (R2)
46	896 vvw	899 (2)	944 (4)	904	δ C(3)C(4)O(5) + δ CCH (R1)
47	883 w	883 (10)	926 (4)	887	γ C–H (R2)
48	–	–	912 (1)	874	γ C–H (R1)
49	866 w	868 (7)	903 (16)	865	δ C(3)C(2)C(1) + δ COC (R1)
50	832 vvw	–	878 (21)	841	δ O(10)C(9)N(11) + δ C(2)C(3)C(4)
51	820 vvw	–	858 (5)	822	γ C–H (R1)
52	–	–	857 (<1)	821	γ C–H (R2)
53	799 vvw	798 (7)	829 (9)	794	δ C(25)C(27)C(23) + δ C(20)C(17)N(15)
54	783 m	781 (1)	779 (73)	746	ν C(13)=S(14)
55	774 m	774 (1)	773 (83)	741	γ C=O + γ N(15)–H
56	758 w	–	767 (21)	735	γ C–H (R1)
57	747 m	750 (16)	748 (3)	717	δ O(10)C(9)C(4) + γ C–H (R2)
58	709 m	710 (3)	730 (28)	699	γ N(15)–H
59	685 m	–	712 (48)	682	γ CCC (R2)
60	629 vw	623 (3)	670 (69)	642	γ N(11)–H
61	605 vw	606 (1)	635 (<1)	608	δ C(21)C(23)C(27) + δ C(20)C(22)C(25)
62	594 w	594 (3)	625 (<1)	599	γ N(11)C(13)N(15) + γ OCC (R1)
63	–	588 sh	512 (8)	586	δ N(15)C(17)C(20)
64	573 vvw	573 (3)	606 (22)	581	γ CCC (R1)
65	–	567 (1)	599 (<1)	574	γ CCC (R1)
66	513 vw	513 (3)	575 (16)	551	δ C(13)N(15)C(17)
67	448 vw	–	517 (18)	495	δ C(4)C(9)N(11)
68	415 vw	–	478 (5)	458	γ CCC (R2)
69	–	–	413 (<1)	396	γ CCC (R2)
70	–	356 (3)	392 (2)	376	τ CCCC (R2)
71	–	311 (9)	354 (12)	339	δ C(9) N(11)C(13)
72	–	295 (7)	305 (8)	292	δ C(3)C(4)C(9)
73	–	258 (6)	298 (<1)	285	τ CCCC (R2) + τ CCCC (R1)

Table 7 (continued)

Mode	Experimental		Calculated[c]		Tentative assignment[d,e]
	IR[a]	Raman[b]	Unscaled	Scaled	
74	–	222 (11)	227 (17)	217	τ C(13)–N(11)
75	–	207 (11)	213 (3)	204	τ C(9)N(11)
76	–	–	184 (2)	176	τ CCCC (R1)
77	–	–	166 (<1)	159	τ CCCC (R2)
78	–	–	125 (5)	120	τ C(9)C(4)
79	–	–	95 (1)	91	τ COCC (R1)
80	–	–	66 (2)	63	τ CCOC (R1)
81	–	–	52 (1)	50	τ C(13)–N(15)
82	–	–	24 (1)	23	τ CCCC (R2)
83	–	–	19 (<1)	18	τ C(17)C(20) (R2)
84	–	–	12 (1)	11	τ C(17)–N(15)

[a] sh, shoulder; s, strong; w, weak; m, medium; v, very.
[b] Relative band heights in parentheses.
[c] Calculated at B3LYP/6-311++G(d,p) level of theory. IR intensities are shown in parenthesis.
[d] v: stretching, δ: in-plane deformation, γ: out-of-plane deformation, ρ: rocking, ω: wagging, $\tau\omega$: twisting, τ: torsion modes.
[e] See Fig. 1 for the atoms numbering scheme. R1: furan ring; R2: benzene ring.

at 2914 cm^{-1} is assigned to the symmetric stretching mode. This mode is observed in the Raman spectrum at 2916 cm^{-1}. These values are in agreement with the values calculated theoretically.

The band observed in the IR spectrum at 1450 cm^{-1} (1452 cm^{-1} in Raman) is assigned to the CH$_2$ bending mode. This band was predicted at 1487 cm^{-1} in the calculated spectrum. The weak band observed at 1367 cm^{-1} in the IR spectrum is assigned to the CH$_2$ wagging mode. The bands corresponding to the twisting and rocking modes of the methylene group are observed at 1201 and 930 cm^{-1}, respectively in the IR spectrum. These bands are observed at 1202 and 932 cm^{-1} in the Raman spectrum of the solid substance.

C–H vibrations. The aromatic C–H stretching vibrations are observed generally between 3100 and 3000 cm^{-1}[46]. In this region the bands are not affected appreciably by the nature of substituents. The aromatic C–H stretching vibrations present in the benzene ring appear as very weak bands in the IR spectrum located at 3138, 3125, 3113 and 3100 cm^{-1}. In the Raman spectrum, the bands corresponding to the mentioned mode appear at 3135, 3129, 3115 and 3103 cm^{-1}. The aromatic C–H in-plane bending modes of benzene and its derivates are observed in the region 1400–1000 cm^{-1}. The bands observed at 1426, 1320, 1154 and 1019 cm^{-1} in the IR spectrum are assigned to the aromatic C–H in-plane bending mode. The aromatic C–H out-of-plane bending modes appear in the IR spectrum as weak bands located at 966, 956 and 883 cm^{-1} and in Raman at 966, 959 and 883 cm^{-1}.

One characteristic of the five-membered rings is that the ring = CH stretch bands have somewhat higher frequencies than those in six-membered ring analogues, which generally appear at 3100–3000 cm^{-1} [46]. The bands located at 3221, 3211 and 3168 cm^{-1} in the IR spectrum (3225, 3206 and 3165 cm^{-1} in Raman) are assigned to the C–H stretching vibrations of the furan ring.

C=O group modes. The carbonyl group is contained in a large number of different classes of compounds such as aldehydes, ketones, carboxylic acids, esters, amides, etc., for which a strong absorption band attributed to the C–O stretching vibration, is observed in the region between 1850 and 1550 cm^{-1}. The stretching vibration of C=O group is observed as a strong band in the IR spectrum at 1666 cm^{-1}. This band appears in the Raman spectrum as a band located at 1665 cm^{-1}. The very weak band observed at 832 cm^{-1} in the IR spectrum is assigned to the C=O in-plane bending mode. The medium intensity band observed in the IR spectrum at 774 cm^{-1} is assigned to the out-of-plane C=O

bending mode. These values are in agreement with calculations performed with the B3LYP method (see Table 7) and in literature [43–46].

C=S group modes. Generally, in thioureas, the band corresponding to the C=S stretching vibration appears between 800 and 600 cm^{-1} [42]. The medium intensity band observed in the IR spectrum at 783 cm^{-1} is assigned to the C=S stretching mode. This band appears at 781 cm^{-1} in the Raman spectrum. According to the calculations performed at B3LYP/6-31++G(d,p) level, the band corresponding to this mode appears at 779 cm^{-1} (see Table 7). The band corresponding to the N–C–N bending mode appears as a weak band in the IR spectrum at 594 cm^{-1}. The IR spectrum of the title compound does not display the S–H stretching mode at about 2600 cm^{-1} indicating that that this compound remains in the thio keto-amine form in solid state [45].

Skeletal stretching modes. The C–C stretching vibrations are more interesting if the double bond is in conjugation with the ring. The C–C stretching modes generally appear as bands in the range 1650–1200 cm^{-1}. The bands located at 1582, 1272 and 1162 cm^{-1} in the IR spectrum (1584, 1557, 1273 and 1162 cm^{-1} in Raman) are assigned to the C–C stretching mode of the benzene ring. The bands corresponding to the C–C stretching modes of the furan ring appear at 1550, 1472 and 1234 cm^{-1} in the IR spectrum (1545, 1474 and 1236 cm^{-1} in Raman). The bands observed at 971, 799 and 605 cm^{-1} in the IR spectrum are assigned to the CCC in-plane bending mode and the bands located at 685 and 415 cm^{-1} in the IR spectrum are assigned to the CCC out-of-plane bending mode of the benzene ring.

The identification of the C–N stretching vibration generally is very difficult to identify due to the fact that in this region several modes are mixed. The C–N stretching vibration coupled with scissoring of N–H and C–C is moderately to strong active in the region between 1330 and 1220 cm^{-1} [46]. In the present investigation, the C–N stretching modes are observed at 1330 and 1089 cm^{-1} in the IR spectrum and at 1328 and 1089 cm^{-1} in Raman. The experimental values of C–N stretching modes show good agreement with theoretical values. The corresponding calculated frequencies are 1366 and 1130 cm^{-1}.

Conclusions

In this work, a complete structural, thermodynamic, vibrational and electronic investigation along with UV–visible, FTIR, Raman, NBO analysis and AIM approach of the thiourea derivate 1-

benzyl-3-(2-furoyl) thiourea have been carried out with B3LYP methods and different basis sets. The calculated IR and Raman spectra are compared with the previously reported ones. A complete assignment of the observed bands was possible form the calculated normal modes of vibration. The molecular geometry parameters, bond lengths, angles and torsional angles have been calculated and correlated with the experimental values reported previously through XRD structural study. The geometrical parameters of the title compounds calculated are in good agreement with the XRD results. The intra-molecular hydrogen interaction and ellipticity studied by AIM approach show weak hydrogen interactions and π-character of bond in the aromatic ring. Using NBO analysis the stability of the molecule arising from hyperconjugative interaction and charge delocalization has been analyzed. The energy value of the interaction π^* C(9)–O(10) → π^* C(3)–C(4) is 123.1 kcal mol^{-1} indicating that this interaction produces a great stabilization in the molecule. The TD-DFT calculation assisted the assignment of electronic transitions observed in the UV–visible absorption spectrum. The HOMO is primarily composed of C(17), N(15), S(14), N(11), O(10) and C(20) and C(27) corresponding to the benzene ring. The LUMO is spread over the entire molecule except on the C atoms of the benzyl group. The HOMO–LUMO energy gap is calculated to be 3.865 eV. The low HOMO–LUMO band gap indicates that the title compound is more reactive and less stable. The IR and Raman spectra were obtained and most of the normal modes of vibration were assigned supported by quantum chemical calculations.

Acknowledgements

Appendix A. Supplementary data

Supplementary data associated with this article can be found, in the online version, at http://dx.doi.org/10.1016/j.saa.2015.02.071.

References

[1] D.G. Patil, M.R. Chedekel, J. Org. Chem. 49 (1984) 997.
[2] O. Estévez-Hernández, E. Otazo-Sánchez, J.L. Hidalgo-Hidalgo de Cisneros, I. Naranjo-Rodríguez, E. Reguera, Spectrochim. Acta 62 (2005) 964.
[3] H. Ghosh, Synlett (2009) 2882.
[4] A. Saeed, U. Florke, M.F. Erben, J. Sulfur Chem. 35 (2014) 318.
[5] F.A. Saad, Spectrochim. Acta 128 (2014) 386.
[6] W. Henderson, R.D.W. Kemmitt, S. Mason, M.R. Moore, J. Fawcett, D.R. Russel, Dalton Trans. (1992) 59.
[7] M. Lipowska, B.L. Hyes, L. Hansen, A. Taylor, L.G. Marzilli, Inorg. Chem. 35 (1996) 4227.
[8] E. Otazo-Sánchez, P. Ortiz del Toro, O. Estévez-Hernández, L. Pérez Marín, I. Goicoechea, A. Cerón Beltran, J.R. Villagómez-Ibarra, Spectrochim. Acta A 58 (2002) 2281.
[9] V. Carcu, M. Negoiu, T. Rosu, S. Serban, J. Therm. Anal. Calorim. 61 (2000) 935.
[10] D. Gambino, E. Kremer, E.J. Baran, Spectrochim. Acta 58 (2002) 3085.
[11] Y.F. Yuan, J.T. Wang, M.C. Gimeno, A. Laguna, P.G. Jones, Inorg. Chim. Acta 324 (2001) 309.
[12] B.K. Kaymakcioglu, S. Rollas, E. Korcegez, F. Aricioglu, Eur. J. Pharm. Sci. 26 (2005) 97.
[13] S. Saeed, N. Rashid, P.G. Jones, M. Ali, R. Hussain, Eur. J. Med. Chem. 45 (2010) 1323.
[14] Z. Zhong, R. Xing, S. Liu, L. Wang, S.B. Cai, P.C. Li, Carbohydr. Res. 343 (2008) 566.
[15] O. Estévez-Hernández, E. Otazo-Sánchez, J.L. Hidalgo-Hidalgo de Cisneros, I. Naranjo-Rodríguez, E. Reguera, Spectrochim. Acta A 64 (2006) 961.
[16] H. Pérez, Y. Mascarenhas, O. Estévez-Hernández, S. Santos, J. Duque, Acta Crystallogr. E 64 (2008) o695.
[17] M.J. Frisch, J.A. Pople, J.S. Binkley, J. Chem. Phys. 80 (1984) 3265;
M.J. Frisch, G.W. Trucks, H.B. Schlegel, G.E. Scuseria, M.A. Robb, J.R. Cheeseman, J.A. Montgomery Jr., T. Vreven, K.N. Kudin, J.C. Burant, J.M. Millam, S.S. Iyengar, J. Tomasi, V. Barone, B. Mennucci, M. Cossi, G. Scalmani, N. Rega, G.A. Petersson, H. Nakatsuji, M. Hada, M. Ehara, K. Toyota, R. Fukuda, J. Hasegawa, M. Ishida, T. Nakajima, Y. Honda, O. Kitao, H. Nakai, M. Klene, X. Li, J.E. Knox, H.P. Hratchian, J.B. Cross, C. Adamo, J. Jaramillo, R. Gomperts, R.E. Stratmann, O. Yazyev, A.J. Austin, R. Cammi, C. Pomelli, J.W. Ochterski, P.Y. Ayala, K. Morokuma, G.A. Voth, P. Salvador, J.J. Dannenberg, V.G. Zakrzewski, S. Dapprich, A.D. Daniels, M.C. Strain, O. Farkas, D.K. Malick, A.D. Rabuck, K. Raghavachari, J.B. Foresman, J.V. Ortiz, Q. Cui, A.G. Baboul, S. Clifford, J. Cioslowski, B.B. Stefanov, G. Liu, A. Liashenko, P. Piskorz, I. Komaromi, R.L. Martin, D.J. Fox, T. Keith, M.A. Al-Laham, C.Y. Peng, A. Nanayakkara, M. Challacombe, P.M.W. Gill, B. Johnson, W. Chen, M.W. Wong, C. González, J.A. Pople, Gaussian 03, Revision C.02, Gaussian, Inc., Wallingford, CT, 2004.
[18] A.D. Becke, J. Chem. Phys. 98 (1993) 5648.
[19] C. Lee, W. Yang, R.G. Parr, Phys. Rev. B 37 (1988) 785.
[20] M.J. Frisch, A.B. Nielsm, A.J. Holder, Gaussview User Manual, Gaussian, Pittsburgh, 2008.
[21] V. Krishnakumar, G. Keresztury, T. Sundius, R. Ramanamy, J. Mol. Struct. 702 (2004) 9.
[22] E.D. Glendening, J.K. Badenhoop, A.D. Reed, J.E. Carpenter, F.F. Weinhold, Theoretical Chemistry Institute, University of Wisconsin, Madison, WI, (1996).
[23] R.F.W. Bader, Atoms in Molecules, A Quantum Theory, Claderon press, Oxford, 1990.
[24] H. Roohi, A. Ebrahimi, F. Alirezapoor, M. Hadealirezahi, Chem. Phys. Lett. 409 (2005) 212.
[25] D.M. Gil, M.E. Tuttolomondo, A. Ben Altabef, Spectrochim. Acta A 123 (2014) 290.
[26] M. Rocha, A. Di Santo, J.M. Arias, D.M. Gil, A. Ben Altabef, Spectrochim. Acta A 136 (2015) 635.
[27] D.M. Gil, O.E. Piro, G.A. Echeverría, M.E. Tuttolomondo, A. Ben Altabef, Spectrochim. Acta A 116 (2013) 122.
[28] M.E. Defonsi Lestard, R.A. Cobos Picot, M.E. Tuttolomondo, A. Ben Altabef, Vib. Spectrosc. 65 (2013) 124.
[29] F. Biegler-Köning, J. Schönnbohn, D. Bayles, J. Comput. Chem. 22 (2001) 545.
[30] U. Koch, P.L.A. Popelier, J. Phys. Chem. 99 (1995) 9747.
[31] W. Koch, G. Frenking, J. Gauss, D. Cremer, J.R. Collins, J. Am. Chem. Soc. 109 (1987) 5917.
[32] I. Rozas, I. Alkorta, J. Elguero, J. Am. Chem. Soc. 122 (2000) 11154.
[33] E. Scrocco, J. Tomasi, Adv. Quantum Chem. 11 (1979) 115.
[34] F.J. Luque, J.M. Lopez, M. Orozco, Theor. Chem. Acc. 103 (2000) 343.
[35] H. Kobinyi, G. Folkers, Y.C. Martin, 3D QSAR in Drug Design, Recent Advances, vol. 3, Kluwer Academic Publishers, 1998.
[36] S. Moro, M. Bacilieri, C. Ferrari, G. Spalutto, Curr. Drug Discov. Technol. 2 (2005) 13.
[37] E. Kavitha, N. Sundaraganesan, S. Sebastian, M. Kurt, Spectrochim. Acta A 77 (2010) 612.
[38] V. Arjunan, L. Devi, R. Subbalakshmi, T. Rani, S. Mohan, Spectrochim. Acta A 130 (2014) 164.
[39] O.A. El-Gammal, T.H. Rakha, H.M. Metwally, G.M. Abu El-Reash, Spectrochim. Acta A 127 (2014) 144.
[40] C. Sridevi, G. Shanthi, G. Velraj, Spectrochim. Acta A 89 (2012) 46.
[41] T.A. Koopsmans, Physica 1 (1993) 104.
[42] R.J. Parr, L.V. Szentpaly, S. Liu, J. Am. Chem. Soc. 121 (1999) 1922.
[43] N. Sundaraganesan, S. Ilakiamani, H. Saleem, P.M. Wojciechowski, D. Michalska, Spectrochim. Acta A 61 (2005) 2995.
[44] R. Raju, C. YohannanPanicker, P.S. Nayak, B. Narayana, B.K. Sarojini, C. Van Alsenoy, A.A. Al-Saadi, Spectrochim. Acta A 134 (2015) 63.
[45] M. Atiş, F. Karipcin, B. Sariboğa, M. Taş, H. Çelik, Spectrochim. Acta A 98 (2012) 290.
[46] D. Lin-Vien, N.B. Colthup, W.G. Fateley, J.G. Grasselli, The Handbook of Infrared and Raman Characteristic Frequencies of Organic Molecules, Academic Press, 1991.